The Impacts of Global Warming on Climate Zone Changes over Asia based on CMIP6 Projections

Jeong-Bae Kim[1], and Deg-Hyo Bae[1*]

1 Department of Civil and Environmental Engineering, Sejong University, Seoul, South Korea

* Corresponding author: Prof. Deg-Hyo Bae (dhbae@sejong.ac.kr)

Address: Department of Civil & Environmental Engineering, Sejong University, 209 Neungdong-ro, Gwangjin-Gu, Seoul 05006, South Korea

Key Points:

- Potential global warming based on CMIP6 causes the significant changes in regional climates and consequently climate shifts over Asia.
- Pace of climate zone shifts will become faster as the global warms, but the differences exist among the regional climate features.
- Characteristics of climate shifts are more sensitive to the degree of global mean temperature increase than the type of SSP scenarios.

Abstract

It is challenging to estimate how the regional climate will be shifted under future global warming. To reduce the potential risk of regional climate shift under future climates, examining the change in climate features over Asia is important, as approximately 60 percent of the world's population resides there. In this study, climate shifts are assessed over the Asian monsoon region under global mean temperature warming targets from 1.5 °C to 5.0 °C above preindustrial (PI) levels based on different shared socioeconomic pathway (SSP) scenarios. Global warming impacts the individual climate variables, and consequently, it impacts the regional climate features across the Asia region. Temperature change patterns are more dominant contributors to the spatial extent and magnitude of climate shifts than precipitation change patterns. Changes in regional climates show different behaviors according to the degree of global warming rather than the type of SSP scenario. Climate shifts are intensified under a higher level of global warming that is above the PI levels. The largest climate shifts in this region are shown under global warming of 5.0 °C based on the SSP5-8.5 scenario, especially in current polar climate zones. Future change patterns in individual climate zone can differ. Regions with tropical climates and arid climates are likely to be expanded, whereas some regions with warm temperate climates, cold climates, and polar climates are likely to shrink under global warming conditions. Therefore, this study supports the necessity of mitigating greenhouse gas (GHG) emissions and establishing an adaptation plan for future global warming conditions.

Keywords

climate shifts, climate zone, global warming, CMIP6, SSPs, Asia

1 Introduction

Global temperature has increased as a result of enhanced atmospheric greenhouse gases (GHGs) from natural and anthropogenic sources. The gradual long-term global warming trend since the preindustrial (PI) period drives the alteration of Earth's energy cycle, and consequently, it drives the alteration of the climate system with associated impacts (Skalák et al., 2018). Alterations have not only affected extreme climates but also regional climatological features, such as long-term mean temperature and precipitation (IPCC, 2013; 2018). Moreover, future global warming is likely to cause continuous changes in regional climates (Trenberth, 2011; Chevuturi et al., 2018). Many studies have suggested that extreme climate responses to enhanced emission forcings are relatively clear and straightforward (e.g., King and Karoly, 2017; Harrington and Otto, 2018; Li et al., 2018). On the other hand, long-term mean climates are much more obscure at the regional scale (Kim et al., 2020a) because climatology is influenced by local radiative forcings, as well as global circulation effects, such as the advection of air masses from other regions (Paeth et al., 2015). In addition, for each region, climate plays an important role as the primary natural constraint regulating natural and human systems, such as vegetation growth (Nemani et al., 2003), food security (King et al., 2018), water availability, and water-related disasters (Son and Bae, 2015). Therefore, examining the potential changes in regional climates under global warming is needed to address climate variability and changing environmental conditions, especially for the Asia monsoon region, which has the largest population worldwide and is susceptible to climate disasters.

Identifying regional climate features is an essential prerequisite for understanding their response to climate change. Although regional climate characteristics are classified by the homogeneity of several sections (e.g., geography, topography, and ecology), the prevailing approach is climate classification. Climate classification is widely applied due to its relative simplicity concerning input data requirements (Peel et al., 2007; Belda et al., 2014). Thus, this method provides intuitive and valuable insight into the relationships between climate and Earth's physical and biological systems for the current climate, as well as for future climates (Mahlstein et al., 2013) by defining a regional climate type according to the criteria for the long-term mean climate. Therefore, previous studies have suggested that regional climates have shifted under the current climate based on analyses of the changes in the classified climate zone (e.g., Fraedrich et

al., 2001; Chen and Chen, 2013; Belda et al., 2016; Yoo and Rohli, 2016 worldwide; Born et al., 2008 for West Africa; Son and Bae, 2015; Chen et al., 2016 for East Asia)

As global warming increases, examining climate change impacts on climate shifts is among the key scientific issues because shifts in precipitation patterns and increases in temperature are two major components of ongoing climate change (IPCC, 2014). The recent availability of spatially comprehensive long-term datasets from general circulation model (GCM) simulations has made it possible to display of the global spatial extent of climate types over time. Previous studies have established that climate classification depends on the climate classification method under climate scenarios derived from GCM simulations (Rahimi et al., 2020; Xia et al., 2020). In particular, GCMs, which are part of the fifth phase of the Coupled Model Intercomparison Project (CMIP5) (Taylor et al., 2012), have been widely used in recent decades for climate classification. Rubel and Kottek (2010) showed that temperate climate regions are projected to expand, while subpolar and alpine climate regions are projected to shrink significantly in China by 2100. Feng et al. (2014) suggested that the climate tends to shift toward warmer and drier types across the global region, with the largest changes in the Northern Hemisphere being north of 30° N during the 21st century. Talchabhadel and Karki (2019) projected changes in the climate boundary across Turkey for the near (and mid) future period and showed that the degree of climate boundary shifts is higher under RCP 8.5 than under RCP 4.5. Romshoo et al. (2020) analyzed the changes in the distribution of prevalent climate zones across the Indian Himalayan region using 3 emission scenarios for future projections. Climate change is likely to shrink the cold desert climate zone and expand the subtropical and temperate zones, whose features are significant under high radiation forcing. These results indicate that global warming is a major source of climate change shifts worldwide. However, shifting features (e.g., shrinkage or expansion, degree of change) are projected to differ based on existing climate type and radiation forcing scenarios.

The 2015 Paris Agreement established a global framework to avoid catastrophic consequences due to climate change by limiting global warming (United Nations Framework Convention on Climate Change (UNFCCC), 2015). In addition, efforts to keep the increase in global average temperature well below 2.0 °C above preindustrial (PI) levels and to pursue an ambitious increase by 1.5 °C above PI levels are being continued by the UNFCCC since the 2015 Paris Agreement. Based on this background, recent studies have investigated both the

impacts of certain warming targets (i.e., 1.5 and 2.0 °C) on climate variables and the benefits of achieving an extra 0.5 °C reduction in global warming (IPCC, 2018). These studies have reported climate responses in the future period. However, these studies are limited in projecting the climate shift under the current degree of global temperature rise and more feasible future conditions.

To the best of our knowledge, only a few studies have analyzed the potential impact of global warming on regional climate shifts (Mahlestein et al., 2013). Additionally, with the sixth phase of the Coupled Model Intercomparison Project Phase (CMIP6; Eyring et al., 2016), the climate model simulations show robust and improved Asian monsoon characteristics based on more complicated physical processes (Gusain et al., 2020). For analyses of the latest CMIP6 outputs, it is possible to suggest updated results and a better understanding of climate shifts over the Asian monsoon region. In this study, we assess the global warming impacts on the regional climate features corresponding to warming targets with a focus on the Asian monsoon region (see Figure 2), as delineated by Kim et al. (2020a). The climate classification method is applied to investigate the regional climate features (e.g., types and spatial boundary) and examine the changes in climate features responding to potential global warming conditions based on multiple ensembles of GCM climate projections. To consider the reliability of future projections, we present the results based on the multimodel ensemble mean (MME) derived from five selected GCM projections, including intermodal agreement. The level of agreement among the multiple projections is used to assess the robustness of climate projections (Tebaldi et al., 2011; Saeed et al., 2018). This study provides valuable information for policymakers to identify changes in regional climate shifts caused by the impacts of anthropogenically induced warming.

2 Data and Methodology

2.1 Study area and observational data collection

The Asian monsoon region located between 9.75°S to 54.75°N latitude and 60.25°E to 149.75°E longitude is selected as the study area to examine the changes in climate zones under different global warming conditions. This study area is sensitive to global warming because it is highly influenced by large-scale climate systems, such as monsoon systems (International Panel on Climate Change (IPCC), 2013). Observational meteorological datasets are required to validate

the performances of the GCM simulations. We select meteorological datasets considering the availability of long-term records (30 years; 1985-2015). We collect precipitation data from the Asian Precipitation-Highly Resolved Observational Data Integration Toward Evaluation of Water Resources (APHRODITE) product (Yatagai et al., 2012). The maximum and minimum temperature data are obtained from gridded forcing datasets provided by the University of Washington (Adam and Lettenmaier, 2003; Adam et al., 2006) for the period of 1985-2005 and Climate Prediction Center (CPC) Global Temperature data provided by the NOAA/OAR/ESRL PSL, Boulder, Colorado, USA (https://psl.noaa.gov/) to extend the recent period (2006-2015). These observational datasets (hereafter "OBS") are gridded at a 0.5° spatial resolution and interpolated to the same grid system as the GCMs. In addition, we collect digital elevation model (DEM) data with a 30 arc second grid resolution to examine the changes in regional climate with their altitude features in this region from the United States Geological Survey (USGS) and then convert it to the same grid system as other datasets.

2.2 Climate change scenarios

In this study, climate change scenarios are driven by 2 GCM outputs (i.e., KACE-1-0-G and UKESM1-0-LL) participating in CMIP6, which show a satisfactory climate simulation performance (Kim et al., 2020b). KMA's Advanced Community Earth system (KACE-1-0-G; KACE) model, which is a coupled climate model (Atmosphere-Ocean-sea Ice-Land; AOIL) and each component of the Earth system model including the number of physical and biogeochemical processes, has been developed by the National Institute of Meteorological Sciences/Korea Meteorological Administration (NIMS/KMA) with KMA-Met Office Hadley Centre collaboration (see details in Lee et al. (2019)). This model appears to capture the mean climatology and the interannual variability in the observed climate. On the other hand, the UKESM1-0-LL (UKESM1) model, in which the physical atmosphere-land-ocean-sea ice model (i.e., HadGEM3-GC3.1) and the Earth system model (i.e., UKESM1) are applied, was developed by the Met Office Hadley Centre. More detailed model configurations for UKESM1 are suggested in Sellar et al. (2019, 2020). The model runs are being performed by the Met Office Hadley Centre and the NIMS-KMA and New Zealand's National Institute of Weather and Atmospheric Research (NIWA). Individual GCM simulations may depend on the choice of a point on the control run with different initial conditions, which can lead to differences in the

resulting climate (Lutz, et al., 2016). Therefore, we collect 3 initial condition ensemble members for each 2 GCM outputs from the KMA for a more robust estimate of individual GCM simulations. Information about the selected GCMs is given in Table 1. The individual GCM dataset is converted to a 0.5° × 0.5° grid using a bilinear interpolation scheme. Then, the multimodel ensemble (MME) scenario approach, which enables us to provide similar results to the observed data compared with the output from only one climate simulation (Xu et al., 2020; Tegegne et al., 2020), is adopted to consider the uncertainty ranges of climate change projections.

Table 1. List of the CMIP6 2 GCMs used in this study

No.	GCMs	Ensemble	Horizontal resolution* (Lon.×Lat.)	Institute, Nation	References
1	KACE-1-0-G	r1i1p1f1, r2i1p1f1, r3i1p1f1	192 × 144	NIMS/KMA, Korea	Lee et al. (2020)
2	UKESM1-0-LL	r13i1p1f2. r14i1p1f2, r15i1p1f2	192 × 144	Met Office Hadley Centre, UK	Sellar et al. (2019)

Our focus is to understand the changes in climate shifts under different global warming environments, such as the degree of global temperature increase and the pace of climate change. To simulate the climate during both historical and future periods, CMIP6 climate projections forced by 2 shared socioeconomic pathways (SSPs) 1-2.6 and 5-8.5 are selected. The temperature response derived from individual GCMs to different SSP scenarios varies, thereby creating a discrepancy in the increasing trend and slope for the global mean temperature. Here, the analysis is based on SSP1-2.6 and SSP5-8.5, which are commonly considered for realistic future projections. SSP1-2.6 and SSP5-8.5 represent the low and high ends of the range of future forcing pathways, respectively. SSP1-2.6 is the scenario in which the world is under sustainability-focused growth and equality. On the other hand, SSP5-8.5 is the scenario in which the world is under rapid and unconstrained growth of economic output and energy use. Because global warming impacts on regional changes in a regional climate under different SSPs are not simple, the results based on two SSPs can provide useful information for identifying the impacts

of global warming on climate shifts from those expected under different SSPs. This finding implies the need for minimum mitigation strategies and adaptation plans according to global warming induced by GHG emissions, as well as those under relatively low-impact SSPs (e.g., SSP1-2.6).

2.3 Determination of global warming periods and bias correction

We determine the reference period corresponding to a global mean temperature increase in the reference period and future periods corresponding to increases from 1.5 °C to 5.0 °C above the temperature during the PI period (1861-1890) under the two SSP scenarios (e.g., SSP1-2.6 and SSP5-8.5) using the time sampling method (James et al., 2017; Sylla et al., 2018; Kim et al., 2020a). In this process, the individual 30-year periods and their central years (i.e., the median year of each period) are determined based on the temperature anomalies relative to the PI period temperature. All GCM ensembles reach specific warming levels in their central years and in the 30-year reference and future periods under both SSP1-2.6 and SSP5-8.5. In this study, for individual climate scenarios, the central year of each period is the first year in which the 30-year running temperature anomaly surpasses the target temperature above the PI period temperature. The temperature anomalies targeted in this study are 0.66 °C for the reference period (1985-2014, denoted as REF), as shown in Figure 1, and five global warming temperatures (e.g., 1.5, 2.0, 3.0, 4.0, and 5.0 °C) for each future period. Thus, the 30-year running global mean temperature is derived from the individual GCMs during the entire simulation period (1880-2100). Unlike the temperature taken from the central year of the PI period (1875), the temperature anomalies are calculated for the entire period. For the reference period, we set a warming level of 0.66 °C, which was derived from the increased global mean temperature between the PI and REF periods using observed global temperatures (e.g., HadCRUT.4.6), as suggested in Figure 1.

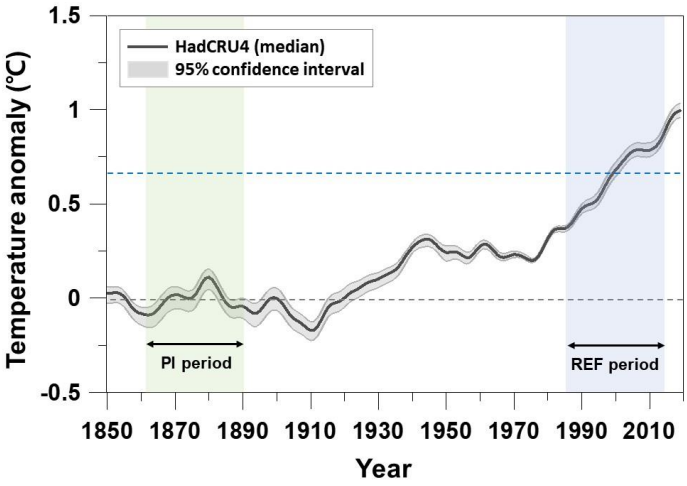

Figure 1. Historical global mean temperature anomalies (unit: °C) relative to the 1861-1890 preindustrial (PI) period based on the observed HadCRU4 temperature data. The thick black solid line and blue dotted line indicate the median value of the 100 ensemble members with the 95% confidence interval (gray range) and the mean value of the 1985-2014 reference (REF) period, respectively.

Figure 2 represents the spreads in the climate simulations derived from 6 ensemble scenarios under the same emission forcing and the central year of each global warming period derived from the MME. Individual ensembles simulate climate based on their own physical climate system processes and initial conditions. Therefore, the central year (and 30-year periods) for each ensemble with global mean temperature increases of 0.66, 1.5, 2.0, 3.0, 4.0, and 5.0 °C based on the two SSPs is determined and applied to the MME approach. As shown in Figure 2, individual global mean temperatures derived from the MME of 6 ensembles are expected to increase by more than 2.0 °C and 5.0 °C by 2100 under SSP1-2.6 and SSP5-8.5, respectively. In addition, there is a shorter time lag between the timing of 1.5 °C and 2.0 °C global warming under SSP5-8.5 (18 years) compared with SSP1-2.6 (16 years).

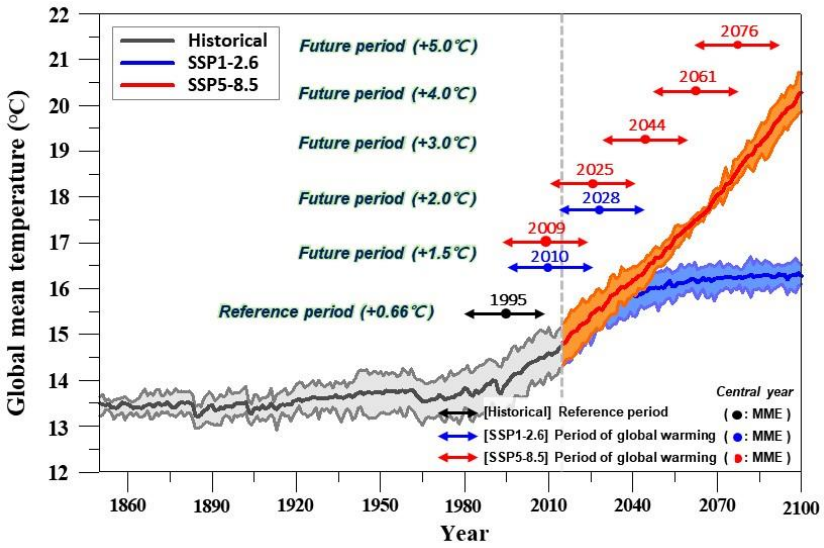

Figure 2. Thirty-year moving averages of the global mean temperature (unit: °C) under SSP1-2.6 and SSP5-8.5. The thick solid lines and shadings indicate the values derived from both MME and the range of the 6 ensemble outputs, respectively. Horizontal arrows indicate the periods of each global warming condition under different SSP scenarios. Closed circles on the lines denote the central year of each global warming period derived from the MME.

All GCMs contain substantial biases in simulating observed climate characteristics in terms of their spatial and temporal scales. To reduce substantial biases in the GCM simulations, we use the quantile mapping method, which is one of the statistical bias correction methods. This method adjusts the whole distribution of two datasets by matching the cumulative distribution function (CDF) of the climate model data to the CDF of the observed data on a daily basis, thereby improving the mean, variance, and extreme values. The method is an effective and simple way to correct the systemic biases in climate simulations; therefore, it is widely used for climate models (MacDonald et al., 2018; Kim et al., 2020a).

2.4 Classification of climate zone

To classify the climate zone over the Asian monsoon region, we apply Köppen's climate classification method (Köppen, 1936). This method is widely used to identify regional climates based on their precipitation and temperature patterns because the method is universal in its usage and simplicity (Belda et al., 2014). First, each subregion is categorized into five main climate

zones according to the climate boundary conditions: tropical climate (A), arid climate (B), warm temperate climate (C), snow climate (D), and polar climate (E); these zones are based on threshold values of monthly temperature and precipitation (e.g., temperatures for climate zones A, C, D, and E; moisture availability is required for plant growth in climate zone B). Next, individual subregions represented by capital letters are subdivided with second letters based on the temperature feature for the E climate or precipitation feature (e.g., their seasonality or degree of dryness) for the other 4 main climates. A detailed description of the Köppen climate classification is listed in Table 2.

Table 2. The description and distribution rate of the identified climate zone over the Asian monsoon region derived from the OBS and MME for the historical period (1985-2014) based on the Köppen climate classification method. (Tmin(max): monthly averaged minimum (maximum) temperature, Pmin: monthly averaged minimum precipitation, PANN: annual averaged precipitation, Psmin(smax): minimum (maximum) precipitation in the summer season, Pwmin(wmax): minimum (maximum) precipitation in the winter season, and Pth: dryness threshold calculated as a linear function of regional temperature).

Type	Description	Criterion	Ratio of Area (%)	
			OBS	MME (Bias)
A	Tropical climate	Tmin ≥ +18 ℃	15.8	15.5 (-0.3)
Af	Rainforest	Pmin ≥ 60 mm	7.0	7.0 (0.0)
Am	Monsoon	Not(Af) & Pmin ≥ 100-PANN/25	1.5	1.5 (0.0)
Aw	Savannah	Not(Af) & Pmin < 100-PANN/25	7.3	7.0 (-0.3)
B	Arid climate	PANN < 10Pth	33.6	34.8 (1.2)
BS	Steppe climate	PANN > 5Pth	17.2	17.1 (-0.1)
BW	Desert climate	PANN ≤ 5Pth	16.4	17.7 (1.3)
C	Warm temperate climate	-3 ℃ < Tmin < +18 ℃	16.6	16.0 (-0.6)
Cs	Warm temperate climate with dry summer	Psmin < Pwmin & Pwmax > 3Psmin & Psmin < 40 mm	0.9	0.8 (-0.1)
Cw	Warm temperate climate with dry winter	Pwmin < Psmin & Psmax > 10Pwmin	9.1	7.4 (-1.7)
Cf	Warm temperate climate without dry season	Neither Cs nor Cw	6.7	7.8 (1.1)
D	Cold climate	Tmin ≤ -3 ℃	28.8	28.4 (-0.4)
Ds	Cold climate with dry summer	Psmin < Pwmin & Pwmax > 3Psmin & Psmin < 40 mm	0.9	1.1 (0.2)
Dw	Cold climate with dry winter	Pwmin < Psmin & Psmax > 10Pwmin	16.0	15.8 (-0.2)
Df	Cold climate without dry season	Neither Ds nor Dw	11.9	11.5 (-0.4)
E	Polar climate	Tmax < +10 ℃	5.2	5.3 (0.1)
ET	Tundra climate	0 ℃ ≤ Tmax < +10 ℃	5.2	5.3 (0.1)
EF	Frost climate	Tmax < 0 ℃	0	0 (0.1)

277 # 3 Results and Analysis

278 ## 3.1 Historical climate zone in Asia

279 Evaluation of GCM ensemble simulations through comparisons with observations is a
280 prerequisite to applying them for climate change impact assessment. First, GCM ensemble
281 projections are validated to examine whether GCM simulations can properly reproduce the
282 historical climatology features shown in the observation datasets. The long-term (e.g., 30 years,
283 1985-2014) annual mean meteorological variables (i.e., precipitation, maximum temperature, and
284 minimum temperature), which are used as inputs for the Köppen climate classification method,
285 are derived from the GCM simulations after bias correction and observational datasets on a
286 monthly time scale at each grid point over the Asian monsoon region. Hereinafter, the results
287 based on the MME of the 6 selected ensembles and the observational data are referred to as the
288 MME and OBS, respectively.

289 Figure 3 shows the spatial distribution of the mean annual precipitation, mean annual
290 maximum temperature, and mean annual minimum temperature from the OBS and MME. As
291 seen in Figure 3a, the MME captures both the spatial pattern and magnitude of annual mean
292 precipitation well (spatial correlation coefficient = 0.99). The MME shows a tendency to slightly
293 overestimate (or underestimate) the OBS annual mean precipitation in Southeast China (or
294 Northeast India); however, there is a similarity in the spatial patterns between the OBS and
295 MME precipitation. Figure 3b (and Figure 3c) shows the validation of the OBS and MME
296 maximum temperature (and minimum temperature). The MMEs of minimum and maximum
297 temperature represent the OBS temperature features (spatial correlation coefficient = 0.99).
298 Based on the results, the MME shows reasonable historical simulations for each climatological
299 variable compared with the OBS. The results indicate the reliability of the climatological
300 responses to the climate forcing derived from the MME, which is derived from the bias-corrected
301 GCM ensembles.

302

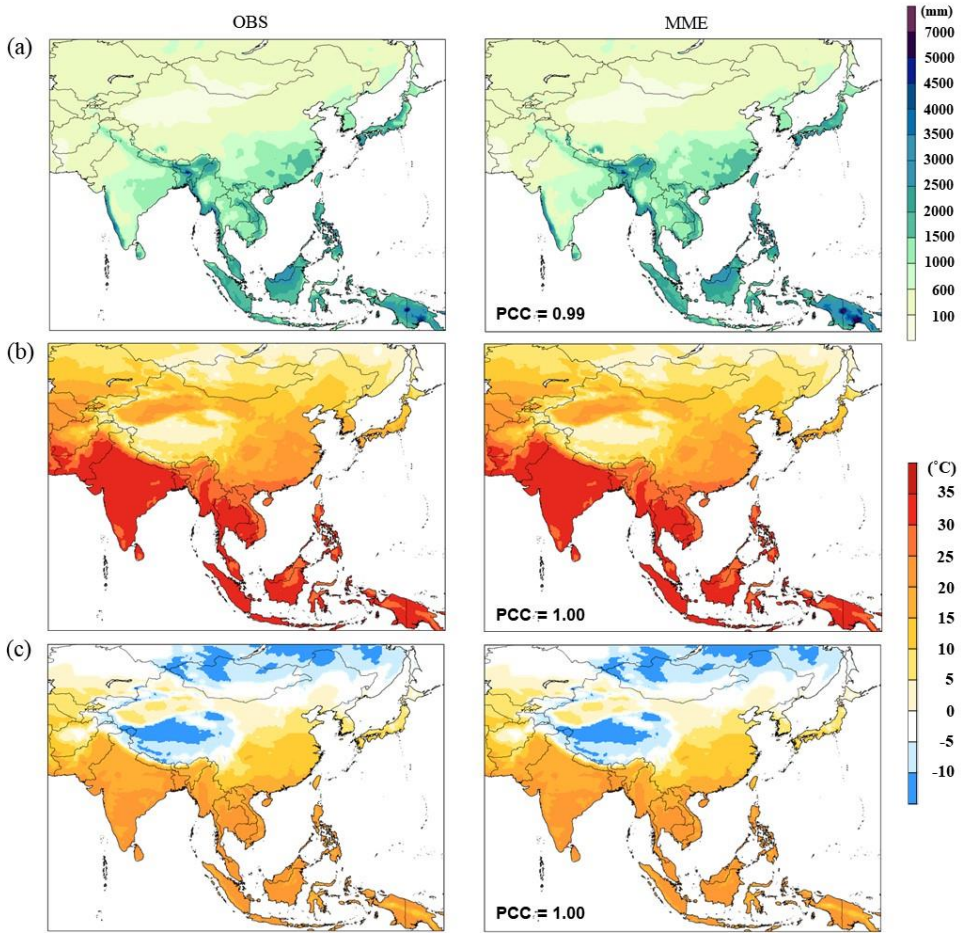

Figure 3. Spatial distributions of the (a) mean annual precipitation (unit: mm), (b) mean annual maximum temperature (unit: °C), and (c) mean annual minimum temperature (unit: °C) for the historical period (1985-2014) in the Asian monsoon region. OBS and MME denote the values obtained from the observational dataset and the MME of bias-corrected outputs from the GCMs, respectively.

Next, classified climate zones over the Asia monsoon region based on the MME for the historical period (1985-2014) are compared with those based on the OBS. Figure 4 shows the spatial distribution of classified climate zones based on the OBS and MME derived from 6 ensemble scenarios for the historical period by applying Köppen's climate classification method. The climate zones in this region are classified into 12 climate zones based on both the OBS and MME. The MME captures the spatial pattern and the extent of the individual climate zone well based on the OBS (spatial correlation coefficient = 0.96). Table 2 shows the percentage of an area corresponding to the individual climate zone derived from the OBS and MME. The

differences in the distribution ratios for the 12 climate zones are relatively small, ranging from -1.3% to 1.7%. The MME adequately simulates the distribution of classified climate zones derived from the OBS.

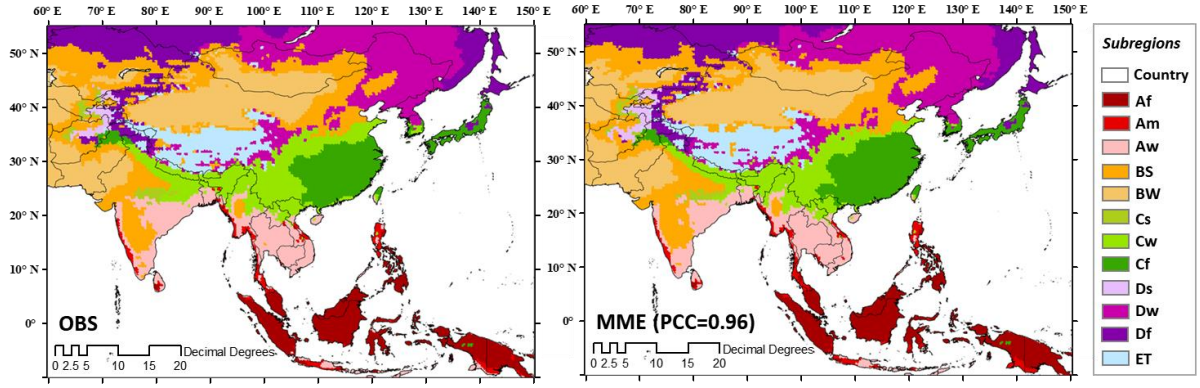

Figure 4. Spatial distributions of the observed and simulated climate zone classifications based on the MME for the historical period (1985-2014) in the Asian monsoon region. OBS and MME denote the values obtained from the observational dataset and the MME of bias-corrected outputs from the GCMs, respectively.

The dominant climate in this region is the arid climate zone (B), followed by the cold climate zone (D), warm temperature climate zone (C), tropical climate zone (A), and tundra climate zone (E). Zone A surrounds low latitudes, such as Indonesia, Malaysia, the Philippines, and Thailand (Aw), the north-central part of Vietnam and the western shoreline of both India and Myanmar (Am; located between Af and Aw), the southern parts of Indonesia, Vietnam, Thailand, the southern and northeastern parts of India and part of Myanmar (Aw; located between 9° N and 25° N). Zone B includes the northwestern part of China, the north-central part of India, some parts of Mongolia, Pakistan, and Afghanistan, and the southern part of Kazakhstan (BS), as well as northern China, southern Mongolia, and some parts of Pakistan and Kazakhstan (BW). Zone C appears in some parts of India and Afghanistan (Cs), the southern and eastern parts of China, the northern parts of India, Vietnam and Myanmar, and the southern part of South Korea (Cw), as well as most of southeastern China, the shoreline of South Korea, and the southern part of Japan (Cf). Zone D spreads over the northern part of Afghanistan (Ds), the central part of China at high altitudes, and most of the inland region at high latitudes (Dw and Df) above 38° N. Zone ET appears on the Tibetan Plateau and the Himalayas at high altitudes.

To classify the climate zone over the Asian monsoon region, we apply Köppen's climate classification method (Köppen, 1936). This method is widely used to identify regional climates based on their precipitation and temperature patterns because the method is universal in its usage and simplicity (Belda et al., 2014). First, each subregion is categorized into five main climate zones according to the climate boundary conditions: tropical climate (A), arid climate (B), warm temperate climate (C), snow climate (D), and polar climate (E); these zones are based on threshold values of monthly temperature and precipitation (e.g., temperatures for climate zones A, C, D, and E; moisture availability is required for plant growth in climate zone B). Next, individual subregions represented by capital letters are subdivided with second letters based on the temperature feature for the E climate or precipitation feature (e.g., their seasonality or degree of dryness) for the other 4 main climates. A detailed description of the Köppen climate classification is listed in Table 2.

3.2 Global warming impacts on potential climate shifts in Asia

In this section, we examine the future changes in the classified climate zone over Asia under global mean temperature (GMT) increases from 1.5 °C to 5.0 °C compared with the reference global warming temperature levels based on the two SSPs (i.e., SSP1-2.6 and SSP5-8.5). Thus, future climate variables are obtained from the MMEs of six ensemble scenarios under specific GMT increases. Under the two selected SSPs, compared with the reference period (i.e., 1985-2014, REF), Figure 5 indicates the timing of specific global warming levels (Figure 5a) and changes in the shifted climate area in the Asia monsoon region corresponding to this timing (Figure 5b). Figure 5a presents the changes in the central year corresponding to individual global warming conditions above the PI level. The MME-based global warming temperature will increase to 2.0 °C and 5.0 °C under SSP1-2.6 and SSP5-8.5 by 2100, respectively. The pace of GMT rise under SSP5-8.5 is much faster than that under SSP1-2.6 and is expected to accelerate as warming intensifies. Figure 5b shows the proportion of areas where the existing climate in an individual grid over the Asian monsoon region changes under global warming conditions. The areas with shifted climates under global warming will increase regardless of the type of SSP. Fewer differences (e.g., less than 0.6% of the area) between the 2 SSPs are found in the rate of change under 1.5 °C and 2.0 °C warming. More specifically, approximately 8.8% (8.2%) and

13.8% (13.2%) of land area across the Asia monsoon region will be expected to undergo a change under 1.5 and 2.0 °C warming in SSP5-8.5 (SSP1-2.6), respectively. Under additional global warming beyond 2 °C, the ratio of the area with a changing climate zone under global warming conditions ranges from 21.7% under 3.0 °C warming (approximately 2040 years) to 32.9% under 5.0 °C warming (approximately 2070 years) in the most pessimistic scenario (SSP5-8.5). This result indicates that the pace of climate shifts increases as the gradual GMT increases due to future climate change, which is in line with the results from Mahlstein et al. (2013). These features reveal that the impacts of global warming are likely to cause regional climate shifts in Asia, consequently threatening the ecosystem and human well-being by altering the existing climate system.

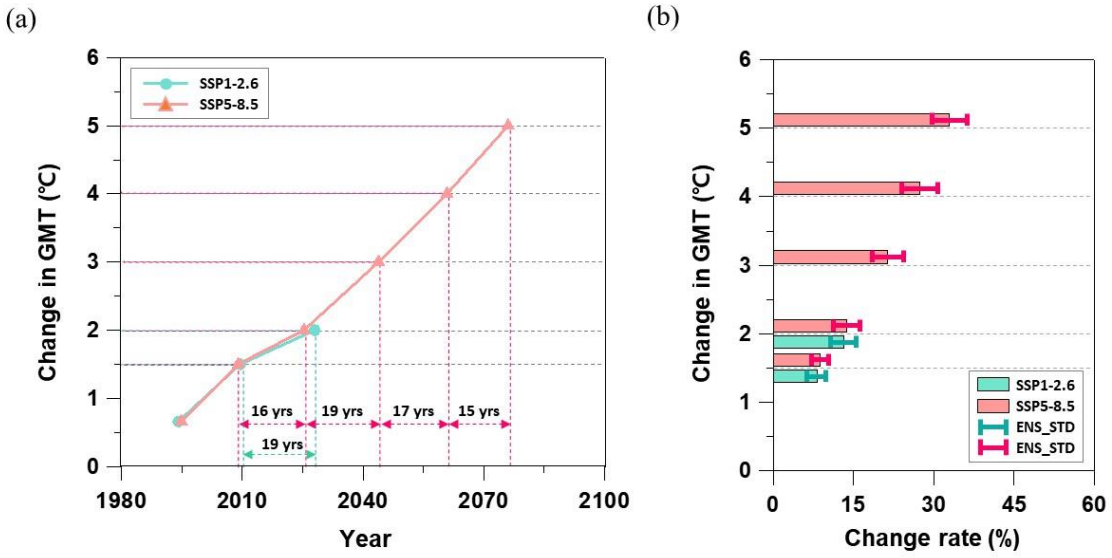

Figure 5. (a) Differences in periods between one and another global warming level (unit: %) forced by SSP1-2.6 (green line with green circles) and SSP5-8.5 (pink line with the pink triangle) based on the MME. (b) Relative area change in the classified climate zones over Asian monsoon regions (unit: %) under global warming levels forced by SSP1-2.6 (green bars) and SSP5-8.5 (pink bars) compared with the reference period (REF). The green (pink) bar in the MME histogram indicates the intermodel spread measured by the 6 bias-corrected ensembles of GCM outputs.

To examine the impact of SSP emission scenarios on climate zone change under global warming levels, we compare the spatial patterns of climate zone change using SSP5-8.5 with those using SSP1-2.6. Figure 6 shows the spatial distributions of the classified climate zone

under 1.5 °C and 2.0 °C of global warming over the Asian monsoon region under SSP5-8.5 with a degree of consistency in the results between SSP1-2.6 and SSP5-8.5. The spatial agreement in the classified climate zone between SSP5-8.5 and SSP1-2.6 is represented by black dots in Figure 6a for 1.5 °C of warming and Figure 6b for 2.0 °C of warming. Despite the disparity in the global warming patterns (e.g., the pace of global warming and the degree of global warming levels by 2100; see Figure 5a) between SSP1-2.6 and SSP5-8.5, there is a similarity in the spatial patterns of the classified climate under 1.5 and 2.0 °C global warming derived from 2 SSPs. Under the same global warming conditions, a high spatial correlation coefficient (SCC > 0.98) is shown in the spatial patterns of the classified climate zones between the results under SSP5-8.5 and those under SSP1-2.6. The discrepancy rate of climate zone change is 2.9 % (3.7 %) of the entire area under 1.5 °C (2.0 °C). This result reveals that the SSP scenarios have no significant impacts on climate zone change compared with the degree of global warming levels.

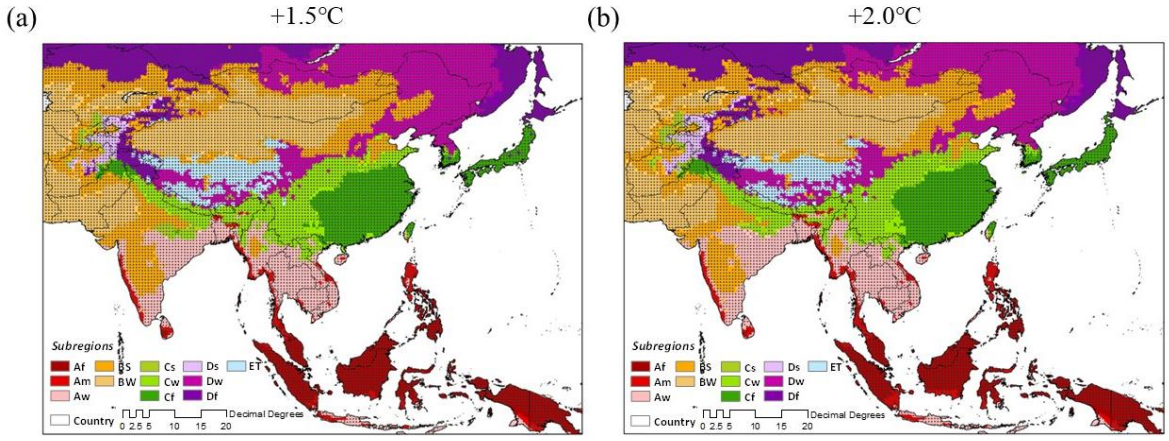

Figure 6. Spatial distributions of the classified climate zone based on the MME and SSP5-8.5 scenarios (a) under 1.5 °C of global warming and (b) under 2.0 °C of global warming over the Asian monsoon region. Black dots denote the agreement of the classified climate zone in an individual grid under the SSP1-2.6 scenario.

3.3 Future projections of shifting in each climate zone

Global warming leads to uneven change patterns that cause the difference in the degree of climate shifts in each climate zone. Therefore, we investigate the changes in individual climate zones under potential warmer conditions. Figure 7b (and Figure 7a) shows the area change in individual climate zones under global warming compared with the REF based on SSP5-8.5 (and

SSP1-2.6). Based on both SSPs, each climate zone shows a different magnitude and trend of change patterns under global warming compared with the REF. As shown in the results under both SSPs, a decreasing area in zone Af and cold climate zones (e.g., Dw, Df, and ET) occur in a warmer world, while an increasing area is shown in zones Am, Aw, and BS. The change patterns of the climate zone in most climate zones are more accelerated under warmer climates except for some climate zones (e.g., zones BW, Cw, Cf, and Ds). More importantly, under 4.0 °C of warming forced by SSP5-8.5, the change signal in each zone shows a large amount of change. Hence, global warming surpassing the 2.0 °C global warming level will lead to tremendous adverse influences on the risk due to climate shifts across the Asian monsoon region.

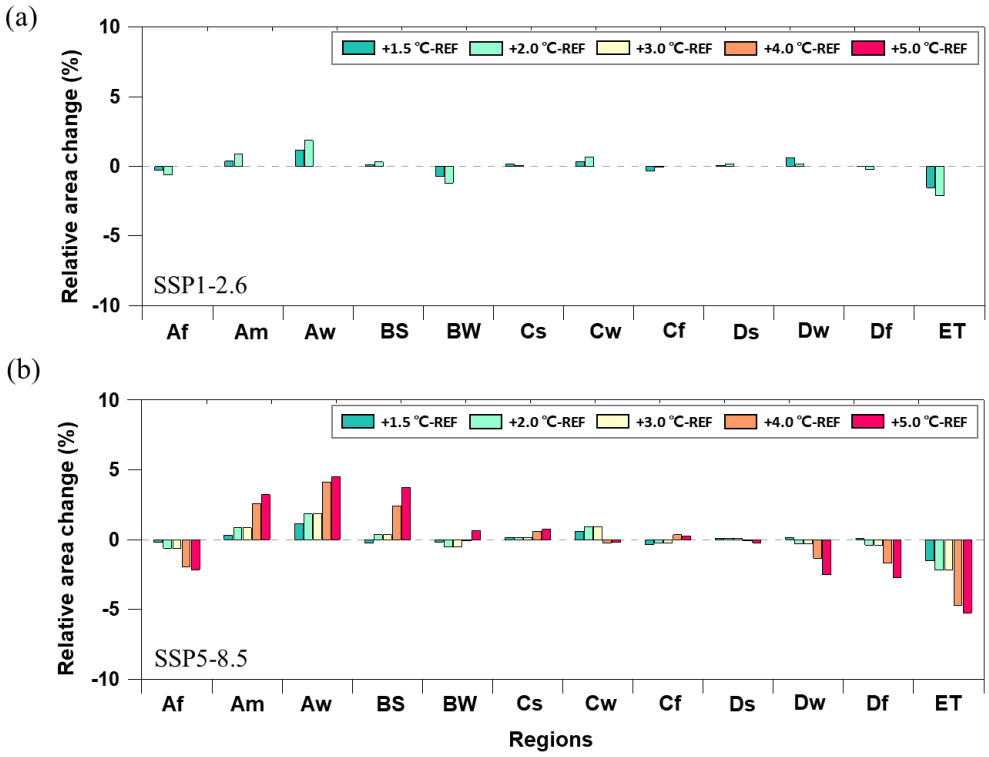

Figure 7. Relative area changes in 12 individual classified climate zones over Asian monsoon regions (unit: %) under global warming levels compared with the reference period derived from the MME forced by (a) SSP1-2.6 and (b) SSP5-8.5.

To consider all possible degrees of global warming above the PI levels, we use the analytical results based on the MME forced by SSP5-8.5. Figure 8 shows when the climate in individual grid points over this study domain is shifted to different climates as a certain temperature rises

(e.g., from 1.5 to 5.0 °C under SSP5-8.5) compared with the REF period. The regions with 4 out of 6 ensemble scenario agreements on the change patterns are identified and employed for the analyses in this figure to provide reliability in the future change patterns. Global warming conditions are expected to change the existing climates in 32.9% of the entire area for the reference period. In general, climate shifts occur in regions with low latitudes (e.g., ranging from 7.75° S to 3.75° S and 20.25° N to 26.75° N) below 2.0 °C of warming. In the warmer world, the regions of changing climates tend to increasingly extend around this area regardless of the type of climate zone.

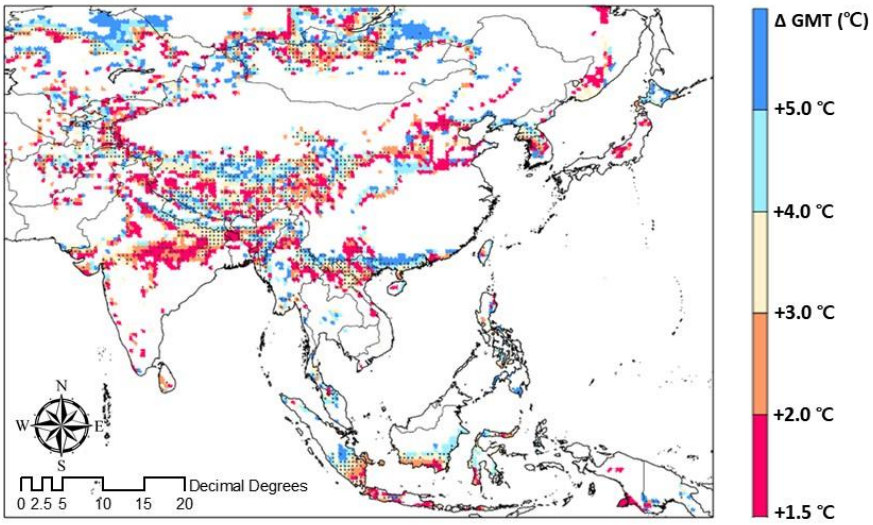

Figure 8. Spatial distributions of the changes in the classified climate zone based on the MME and SSP5-8.5 scenarios under individual global warming levels over the Asian monsoon region. Black dots denote the agreement (i.e., 4 out of 6 ensemble scenarios) in the changes in the classified climate zone in an individual grid.

Figure 9a shows the changes in the distributions of the 5 main climate zones (e.g., zones A, B, C, D, and E) across the Asian monsoon region under a GMT increase in SSP5-8.5. The increasing rate of individual climate zones is calculated based on the entire area change under the REF period. Each climate zone (i.e., zone A) includes subclimate zones (i.e., zones Af, Aw, and Am). Both the A and B climates will increase under global warming conditions. However, the C and D climates tend to decrease under global warming conditions. Climate zones in this study are classified by the precipitation conditions for zone B or by the minimum and maximum temperatures for other zones. For this region, we examine the changes in the climate variable

(e.g., precipitation and temperature) contribute to climate shifts based on the type of shifted climate zone under global warming. Figure 9b represents the box-whisker diagram of the impact factor rate for shifted climate zones under given GMT increases (i.e., from 1.5 to 5.0 °C of global warming). The regional temperature increase has larger impacts on the climate zone than the precipitation increase (see Figure 9b). The areas where climate zone change caused by a precipitation factor (denoted by PRE) occurred increased from 23.3 % at 1.5°C of global warming to 33.5% under 5.0°C of global warming. The areas where the climate zone changes caused by a temperature factor (denoted by TEM) occur decreased from 76.6% at 1.5 °C of global warming to 66.5% at 5.0°C of global warming. This result is because the climate zone shift to C and D from other regions is reduced above 3 °C of global warming. The main driving force of the climate zone shift seems to be a temperature change compared with a precipitation change.

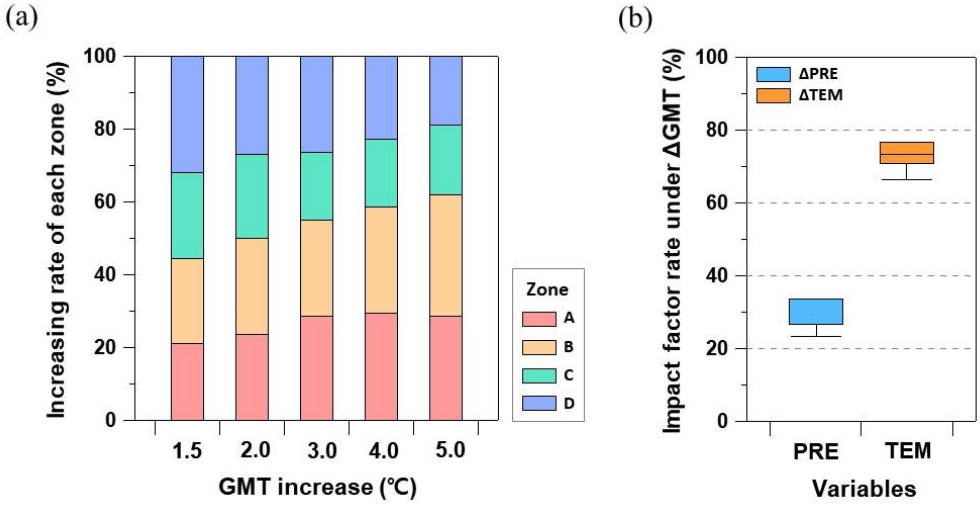

Figure 9. (a) Increasing rate of area (unit: %) corresponding to individual classified climate zones under individual global warming levels based on the MME. (b) Box-whisker plot of relative rate of the impact factor (unit: %) on climate zone change under different global warming levels (e.g., 1.5 °C – 5.0°C) based on the MME and SSP5-8.5.

Consequently, changes in temperature and precipitation are associated with variations in individual climate zones according to potential global warming levels. Figure 10 shows the percentage of the area where the individual climate zone is shifted under GMT increases from 1.5 °C to 5.0 °C compared with the reference period. A small change is suggested in the Aw,

BW, and Cf zones (e.g., less than 12.3%), whereas a large change in the climate zone occurs in the ET, Ds, Dw, and Df zones. Under 5.0 °C of global warming, approximately 97.0% of the ET zone area will shift to other climate zones due to the temperature increase. This finding reveals that ET and D zones with low temperatures are more sensitive to global warming over Asia than other climate zones with warm temperatures. In a warmer world, climate zone shifts are intensified in most climate zones in response to warming as the GMT increases.

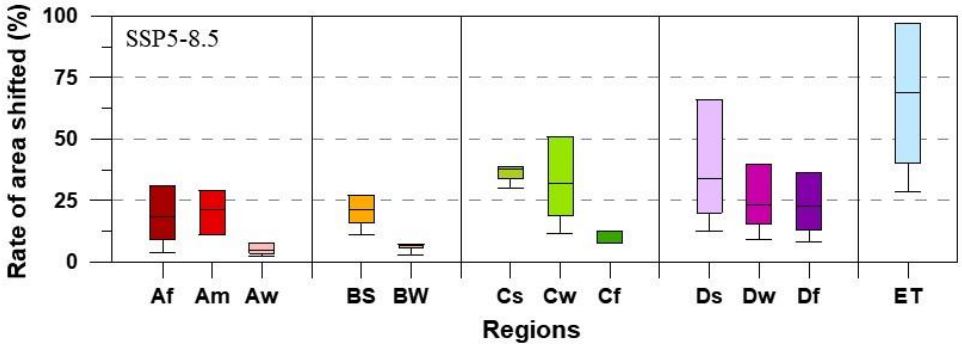

Figure 10. Percentage of area where the individual climate zone shifts under a global mean temperature rise from 1.5 °C to 5.0 °C (unit: %) compared with the reference period (REF).

4 Discussion and Conclusions

Regardless of the region, the global warming caused by the anthropogenic influence impacts on extreme climate events (e.g., heatwaves, maximum precipitation, and flooding) are clear worldwide (IPCC, 2013; 2018). Comparatively, changes in general climates (e.g., long-term mean precipitation) caused by anthropogenic influences are more complex and uncertain in each region. However, there is no doubt that climate change has an impact on regional climates, especially in terms of specific climate features. Therefore, estimating climate shifts is challenging for various sectors because the climate is a fundamentally natural feature related to the ecosystem (e.g., biodiversity loss; extinction of species) and human well-being.

In this study, we focus on identifying the climate zone shift features over the Asia monsoon region in response to various potential GMT increases above the PI level (1861-1890) based on the MME climate projections forced by 2 SSPs and CMIP6 GCM simulations. The periods corresponding to various global warmings (e.g., from 1.5 °C to 5.0 °C) are determined according to the sensitivity of the individual GCMs to the emissions forcing. Several meteorological

variables derived from each climate scenario are applied to the Köppen climate classification after systematic biases in the scenarios are removed by applying quantile mapping. Next, the comparison of the climate shift under different global warming change patterns (e.g., two SSPs) in terms of spatial distribution, shift times, and their characteristics are analyzed based on the MME and intermodel agreement.

The classified climate zone for the historical period (1985-2014) from the MME is similar to the OBS-based distribution of the climate zone over the Asian monsoon region. For the future, the global temperature rise is projected to increase the risk of climate zone shifts over the Asian monsoon region under both SSP scenarios. Additionally, the area of climate zone shift gradually increases as the degree of global temperature rises across this region. This finding supports the concept that global warming accelerates the pace of climate shifts (Mahlstein et al., 2013). However, differences derived from the 2 SSP scenarios in climate shift are relatively smaller under the same global warming conditions. On the other hand, the pace of shifts tends to be largely impacted by the degree of global warming levels regardless of the SSPs. More importantly, under SSP5.8-5, global warming is likely to occur faster, and the degree of warming is much higher (e.g., above 5.0 °C of global warming) than that under SSP1.2-6. These results imply the necessity for mitigation to alleviate the negative impacts of anthropogenic warming and to reduce the increased risk of climate shifts under a much warmer climate.

Figure 11 shows the difference in the period (i.e., Figure 11a) according to the GMT change (e.g., ΔT1-ΔT4) and difference in the magnitude of area change (i.e., Figure 11b) in the climate zone over the Asian monsoon region under increasing GMT conditions. The large variations in terms of warming period are shown under an additional 0.5 °C of warming between 1.5 °C and 2.0 °C (i.e., ΔT1). After ΔT1, the difference in the timing corresponding to changes in GMT tends to be reduced, as shown in Figure 11a, which means that the pace of global warming becomes fast. Under the ΔT1 condition, although the time variation in scenarios forced by SSP5-8.5 is larger than that forced by SSP1-2.6 (see Figure 11a), the ratio of changed area under the SSP1-2.6 scenario is similar to that under the SSP5-8.5 scenario (see Figure 11b). As shown in Figure 11b, the ΔT1 condition will lead to the most significant change in the climate zone over the Asian monsoon region. The increasing rate in the climate zone based on the MME ranges from 5.6% at ΔT4 (i.e., 5.0 °C-4.0 °C) to 7.0% at ΔT2 (i.e., 3.0 °C-2.0 °C). The change in the climate zone shows a large increase in ΔT2. As the global temperature increases, regional

climate change impacts the regional climate in addition to the shifting climate. These results suggest the positive benefits of less warming in terms of climate features. In addition, given the obvious benefits expected by limiting global warming, this study supports the urgency of mitigating GHG emissions in accordance with the 2015 Paris Climate Agreement.

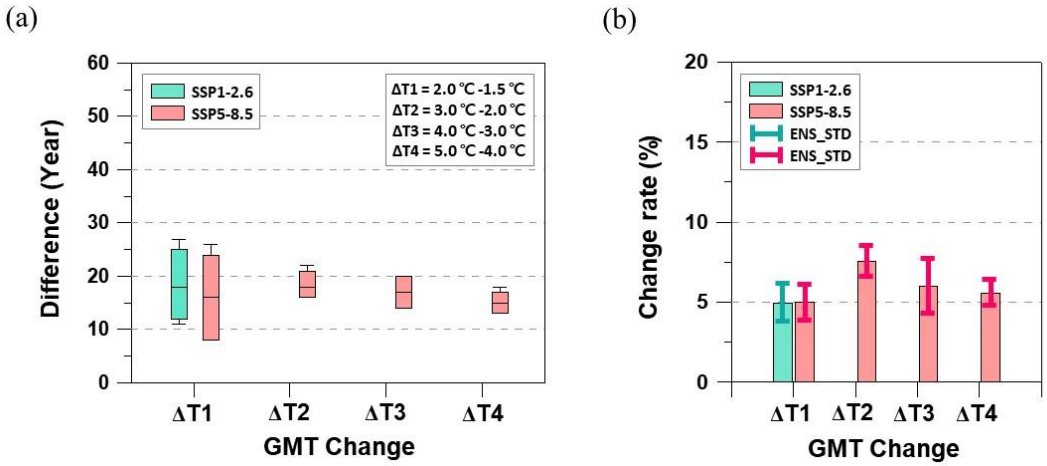

Figure 11. Differences in the (a) period according to the GMT change (i.e., ΔT1-ΔT4). The green (pink) box-whisker plot in (a) indicates the range of periods on the x-axis derived from the 6 ensemble scenarios fed by bias-corrected outputs of the 2 GCMs. (b) Differences in the change rate (unit: %) of the climate zone between one global warming level and the next. The green (pink) bars and error bars with the same color indicate the MME forced by SSP1-2.6 (SSP5-8.5) and the standard deviation of the 6 ensemble scenarios, respectively. In these figures, ΔT1-ΔT4 on the horizontal axis indicates the GMT change.

However, the individual climate zones in this region in response to global warming conditions show different change features (e.g., shrinkage or expansion of each climate zone). Under global warming, arid climates and warm temperature climates are projected to increase, whereas cold climates and polar climates are projected to decrease with a high degree of robustness based on intermodel agreement. This behavior becomes more prevalent under higher temperature increases than under lower temperature increases. Warmer climate conditions tend to alter the climate zone over the Asian monsoon region with an increase in dry and warm climate regions and a reduction in cold climate regions, which are in line with the results from Talchabhadel and Karki (2019) for Nepal and Romshoo et al. (2020) for India. Therefore, a drier and warmer

563 climate over the Asian monsoon region will result in adverse impacts in the context of climate
564 systems, ecosystems, and water resource management.
565

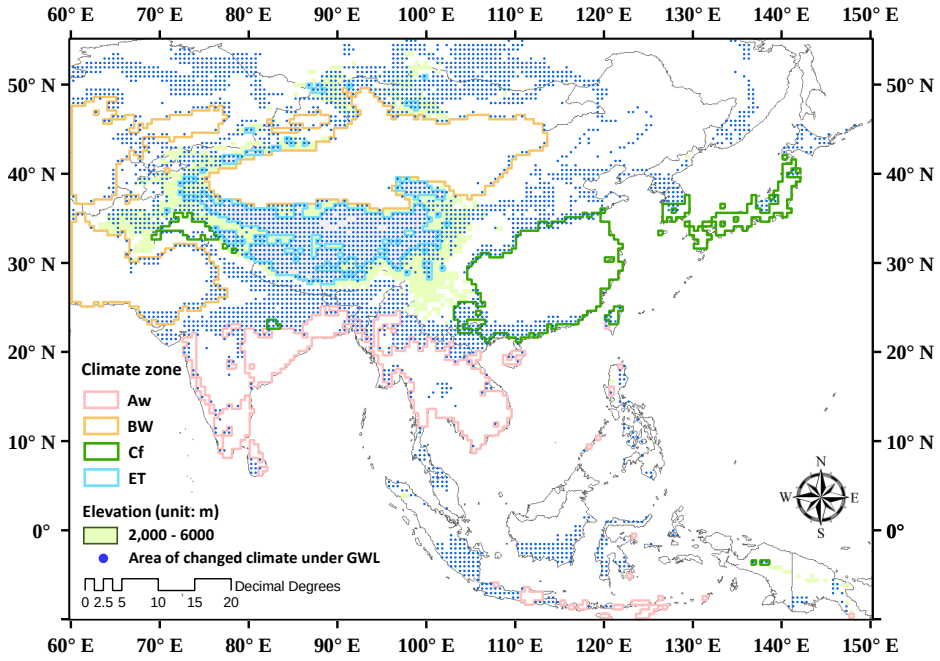

566

567 **Figure 12**. Spatial distributions of the area with changed classified climate zones under global
568 warming levels based on the MME and SSP5-8.5 climate scenarios over the Asian monsoon
569 region. The green shaded area denotes a high altitude (e.g., above 2,000 m) region.

570

571 In addition, the susceptibility of climate shifts under global warming conditions is not uniform
572 in the individual regional climate zones. Figure 12 shows the spatial features of the region where
573 the individual grid point exhibits a climate zone shift under global warming conditions from 1.5
574 to 5.0 °C. Blue dots on the map denote the agreement (i.e., 4 out of 6 ensemble scenarios) on the
575 climate shift occurrence in the individual grid from the existing climate under reference
576 conditions to others under warming conditions. The climate shifts do not tend to be related to
577 latitude features or proximity to the shoreline, but rather, they are related to altitude and the
578 existing climate. As shown in Figure 12, large climate shifts are shown in the region with high
579 altitude (above 2,000 EL.m). Conversely, small climate shifts are shown in the Aw zone (e.g.,
580 delineated in pink), BW zone (e.g., delineated in yellow), and Cf zone (e.g., delineated in green).
581 Although these behaviors are derived from a limited number of GCMs, the level of agreement
582 seen in the six ensemble projections provides a certain level of reliability. In this regard,

583 understanding the changed behavior of the regional climate under a warmer world is necessary to
584 establish a regional climate adaptation plan.

585

586 **Acknowledgments**

587 This work was supported by Korea Environment Industry & Technology Institute(KEITI)
588 through Water Management Research Program, funded by Korea Ministry of
589 Environment(MOE) (130747)

590

591 **Data availability**

592 The CMIP6 data are provided by the National Institute of Meteorological Sciences/Korea
593 Meteorological Administration (NIMS/KMA) from their website
594 (http://www.climate.go.kr/home/CCS/contents_new/35_download.php) or available through
595 ESGF's website (for K-ACE GCMs; https://esgf-node.llnl.gov/search/cmip6/). The
596 meteorological observation data used in this study can be found in the APHRODITE
597 (http://www.chikyu.ac.jp/precip/english/products.html) and global forcing datasets
598 (https://vic.readthedocs.io/en/master/Datasets/Datasets/), and long-term temperature data at the
599 CPC website (https://psl.noaa.gov/). The DEM data (i.e., GTOPO30) are available at USGS ‘s
600 website (https://earthexplorer.usgs.gov/.).

601

602 **References**

603 Adam, J. C., & Lettenmaier, D. P. (2003). Adjustment of global gridded precipitation for
604 systematic bias. *Journal of Geophysical Research,* 108(D9), 1–14.
605 https://doi.org/10.1029/2002JD002499

606 Adam, J. C., Clark, E. A., Lettenmaier, D. P., & Wood, E. F. (2006). Correction of Global
607 Precipitation Products for Orographic Effects. *Journal of Climate,* 19(1), 15-38. https://doi:
608 10.1175/JCLI3604.1

609 Belda, M., Holtanová, E., Halenka, T., & Kalvová, J. (2014). Climate classification revisited:
610 from Köppen to Trewartha. *Climate Research,* 59, 1–13. https://doi.org/10.3354/cr01204

611 Belda, M., Holtanová, E., Kalvová, J., & Halenka, T. (2016). Global warming-induced changes
612 in climate zones based on CMIP5 projections. *Climate Research,* 71(1), 17–31.
613 https://doi.org/10.3354/cr01418
614 Born, K., Fink, A. H., & Paeth, H. (2008). Dry and wet periods in the northwestern Maghreb for
615 present day and future climate conditions. *Meteorologische Zeitschrift,* 17(5), 533–551.
616 https://doi.org/10.1127/0941-2948/2008/0313
617 Chen, D., & Chen, H. W. (2013). Using the Köppen classification to quantify climate variation
618 and change: An example for 1901–2010. *Environmental Development,* 6, 69–79. http://
619 doi.org/10.1016/j.envdev.2013.03.007
620 Chen, T., Zhang, H., Chen, X., Hagan, D. F. Wang, G., Gao, Z., & Shi, T. (2017). Robust drying
621 and wetting trends found in regions over China based on Köppen climate classifications.
622 *Journal of Geophysical Research: Atmospheres*, 122(8), 4228–4237,
623 https://doi.org/10.1002/2016JD026168
624 Chevuturi, A., Klingaman, N. P., Turner, A. G., & Hannah, S. (2018). Projected changes in the
625 Asian-Australian monsoon region in 1.5 °C and 2.0 °C global-warming scenarios. *Earth's*
626 *Future*, 6(3), 339–358. https://doi.org/10.1002/2017EF000734
627 Eyring, V., Bony, S. Meehl, G. A. Senior, C. A., Stevens, B., Stouffer, R. J., & Taylor, K. E.
628 (2016). Overview of the Coupled Model Intercomparison Project Phase 6 (CMIP6)
629 experimental design and organization. *Geoscientific Model Development,* 9(5), 1937–1958.
630 https://doi.org/10.5194/gmd-9-1937-2016
631 Feng, S., Hu, Q., Huang, W., Ho, C. -H., Li, R. and Tang, Z. (2014). Projected climate regime
632 shift under future global warming from multi-model, multi-scenario CMIP5 simulations.
633 *Global and Planetary Change*, 112, 41–52. https://doi.org/10.1016/j.gloplacha.2013.11.002
634 Fraedrich, K., Gerstengarbe, F. -W., & Werner, P. C. (2001). Climate Shifts during the Last
635 Century. *Climatic Change*, 50, 405–441. https://doi.org/10.1023/A:1010699428863
636 Gusain, A., Ghosh, S., & Karmakar, S. (2020). Added value of CMIP6 over CMIP5 models in
637 simulating Indian summer monsoon rainfall. *Atmospheric Research,* 232, 104680.
638 https://doi.org/10.1016/j.atmosres.2019.104680
639 Harrington, L. J., & Otto, F. E. L. (2018). Changing population dynamics and uneven
640 temperature emergence combine to exacerbate regional exposure to heat extremes under

1.5 °C and 2 °C of warming. *Environmental Research Letters,* 13(3), 034011, https://doi.org/10.1088/1748-9326/aaaa99

IPCC. (2013). *Climate Change 2013: The Physical Science Basis.* In T. F. Stocker, et al. (Eds.), Contribution of Working Group I to the Fifth Assessment Report of the Intergovernmental Panel on Climate Change. Cambridge, UK, and New York, NY, USA: Cambridge University Press.

IPCC. (2014). *Summary for policymakers. In: Climate Change 2014: Impacts, Adaptation, and Vulnerability. Part A: Global and Sectoral Aspects.* Field, C. B. et al. (Eds.), Contribution of Working Group II to the Fifth Assessment Report of the Intergovernmental Panel on Climate Change. Cambridge, UK, and New York, NY, USA: Cambridge University Press.

IPCC. (2018). *Global warming of 1.5 °C.* V. Masson-Delmotte, P. Zhai, H. O. Pörtner, D. Roberts, J. Skea, P.R. Shukla, A. Pirani, W. Moufouma-Okia, C. Péan, R. Pidcock, S. Connors, J. B. R. Matthews, Y. Chen, X. Zhou, M. I. Gomis, E. Lonnoy, T. Maycock, M. Tignor, T. Waterfield (Eds.), An IPCC Special Report on the impacts of global warming of 1.5 °C above pre-industrial levels and related global greenhouse gas emission pathways, in the context of strengthening the global response to the threat of climate change, sustainable development, and efforts to eradicate poverty. In Press.

James, R., Washington, R., Schleussner, C.-F., Rogelj, J., & Conway, D. (2017). Characterizing half-a-degree difference: a review of methods for identifying regional climate responses to global warming targets, *WIREs Climate Change,* 8, https://doi.org/10.1002/wcc.457

Kim, J.B., & Bae, D.H. (2020a). Intensification characteristics of hydroclimatic extremes in the Asian monsoon region under 1.5 and 2.0 °C of global warming. *Hydrology and Earth System Sciences,* 24, 5799–5820. https://doi.org/10.5194/hess-24-5799-2020

Kim, M.-K., Yu, D.-G., Oh, J.-S., Byun, Y.-H., Boo, K.-O., Chung, I.-U., Park, J.-S., Par, D.-S., Min, S.-K., & Sung, H.-M. (2020b). Performance evaluation of CMIP5 and CMIP6 models on heatwaves in Korea and associated teleconnection patterns. *Journal of Geophysical Research: Atmospheres,* 125, e2020JD032583. https://doi.org/10.1029/2020JD032583

King, A.D., & Karoly, D. (2017). Climate extremes in Europe at 1.5 and 2 degrees of global warming. *Environmental Research Letter,* 12, 114031. https://doi.org/10.1088/1748-9326/aa8e2c

671 King, M., Altdorff, D., Li, P., Galagedara L., Holden, J., & Unc, A. (2018). Northward shift of
672 the agricultural climate zone under 21st-century global climate change. *Scientific Reports*,
673 8(1), 7904. https://doi.org/10.1038/s41598-018-26321-8
674 Köppen, W. (1936). Das geographische System der Klimate. In: Köppen, W., Geiger, R. (Eds.).
675 Handbuch der Klimatologie. Gebrüder Borntraeger, Berlin.
676 Lee, J., Kim, J., Sun, M.-A., Kim, B.-H., Moon, H., Sung, H.M., Kim, J., & Byun, Y.-H. (2020).
677 Evaluation of the Korea Meteorological Administration Advanced Community Earth-System
678 model (K-ACE). *Asia-Pacific Journal of Atmospheric Sciences*, 56, 381–395.
679 https://doi.org/10.1007/s13143-019-00144-7
680 Li, D., Zhou, T., Zou, L., Zhang, W., & Zhang, L. (2018). Extreme High-Temperature Events
681 Over East Asia in 1.5 °C and 2 °C Warmer Futures: Analysis of NCAR CESM Low-Warming
682 Experiments. *Geophysical Research Letters*, 45, 1541–1550.
683 https://doi.org/10.1002/2017GL076753
684 Lutz, A.F. Maat, H.W. Ter, Biemans, H., Shrestha, A.B., Wester, P., Immerzeel, W.W. (2016).
685 Selecting representative climate models for climate change impact studies: an advanced
686 envelope-based selection approach. *International Journal of Climatology*, 36, 3988–4005.
687 https://doi.org/10.1002/joc.4608
688 MacDonald, M.K., Stadnyk, T.A., Déry, S.J., Braun, M., Gustafsson, D., Isberg, K., & Arheimer,
689 B. (2018). Impacts of 1.5 and 2.0 °C Warming on Pan-Arctic River Discharge Into the
690 Hudson Bay Complex Through 2070. *Geophysical Research Letters*, 45(15), 7561–7570,
691 https://doi.org/10.1029/2018GL079147
692 Mahlstein, I., Daniel, J.S., & Solomon, S. (2013). Pace of shifts in climate regions increases with
693 global temperature. *Nature Climate Change*, 3, 739–743.
694 https://doi.org/10.1038/NCLIMATE1876
695 Nemani, R.R. Keeling, C.D., Hashimoto, H., Jolly, W.M., Piper, S.C., Tucker, C.J., Myneni,
696 R.B., & Running, S.W. (2003). Climate-driven increases in global terrestrial net primary
697 production from 1982 to 1999. *Science*, 300, 1560–1563.
698 https://doi.org/10.1126/science.1082750
699 Paeth, H., Müller, M., & Mannig, B. (2015). Global versus local effects on climate change in
700 Asia. *Climate Dynamics*, 45, 2151–2164. https://doi.org/10.1007/s00382-014-2463-3

Peel, M.C., Finlayson, B.L., and McMahon, T.A. (2007). Updated world map of the Köppen-Geiger climate classification. *Hydrology and Earth System Sciences,* 11, 1633–1644. https://doi.org/10.5194/hess-11-1633-2007

Rahimi, J., Laux, P., & Khalili, A. (2020). Assessment of climate change over Iran: CMIP5 results and their presentation in terms of Köppen–Geiger climate zones. *Theoretical and Applied Climatology,* 141, 183–199. https://doi.org/10.1007/s00704-020-03190-8

Romshoo, S.A., Bashir, J., & Rashid, I. (2020). Twenty-first century-end climate scenario of Jammu and Kashmir Himalaya, India, using ensemble climate models. *Climatic Change,* 162, 1473–1491. https://doi.org/10.1007/s10584-020-02787-2

Rubel, F., & Kottek, M. (2010). Observed and projected climate shifts 1901–2100 depicted by world maps of the Köppen–Geiger climate classification. *Meteorologische Zeitschrift,* 19, 135–141. https://doi.org/10.1127/0941-2948/2010/0430

Saeed, F., Bethke, I., Fischer, E., Legutke, S., Shiogama, H., Stone, D.A., & Schleussner, C.-F. (2018). Robust changes in tropical rainy season length at 1.5 °C and 2 °C. *Environmental Research Letter,* 13, 064024. https://doi.org/10.1088/1748-9326/aab797

Sellar, A. A., Jones, C. G., Mulcahy, J., Tang, Y., Yool, A., Wiltshire, A., et al. (2019). UKESM1: Description and evaluation of the UK Earth System Model. *Journal of Advances in Modeling Earth Systems,* 11, 4513–4558. https://doi.org/10.1029/2019MS001739

Sellar, A.A., Walton, J., Jones, C.G., Wood, R., Abraham, N.L., Andrejczuk, M., et al. (2020). Implementation of U.K. Earth system models for CMIP6. *Journal of Advances in Modeling Earth Systems,* 12, e2019MS001946. https://doi.org/10.1029/2019MS001946

Skalák, P., Farda, A., Zahradníček, P., Trnka, M., Hlásný, T., & Štěpánek, P. (2018). Projected shift of Köppen–Geiger zones in the Central Europe: a first insight into the implications for ecosystems and the society. *International Journal of Climatology,* 38, 1–12. https://doi.org/10.1002/joc.5520

Son, K.H., & Bae, D.H. (2015). Drought analysis according to shifting of climate zones to arid climate zone over Asia monsoon region. *Journal of Hydrology,* 529(3), 1021–1029. https://doi.org/10.1016/j.jhydrol.2015.09.010

Sylla, M.B., Faye, A., Giorgi, F., Diedhiou, A., & Kunstmann, H. (2018). Projected heat stress under 1.5 °C and 2 °C global warming scenarios creates unprecedented discomfort for

731 humans in West Africa. *Earth's Future,* 6, 1029–1044.
732 https://doi.org/10.1029/2018EF000873
733 Talchabhadel, R., & Karki, R. (2019). Assessing climate boundary shifting under climate change
734 scenarios across Nepal. *Environmental Monitoring and Assessment,* 191, 520.
735 https://doi.org/10.1007/s10661-019-7644-4
736 Taylor, K.E., Stouffer, R.J., & Meehl, G.A. (2012). An overview of CMIP5 and the experiment
737 design. *Bulletin of the American Meteorological Society,* 93(4), 485–498,
738 https://doi.org/10.1175/BAMS-D-11-00094.1
739 Tebaldi, C., Arblaster, J.M., & Knutti, R. (2011). Mapping model agreement on future climate
740 projections. *Geophysical Research Letters,* 38(23), L23701,
741 https://doi.org/10.1029/2011GL049863
742 Tegegne, G., Melesse, A.M., & Worqlul, A.W. (2020). Development of multi-model ensemble
743 approach for enhanced assessment of impacts of climate change on climate extremes. *Science*
744 *of The Total Environment,* 704, 12321-12330, https://doi.org/10.1016/j.scitotenv.2019.135357
745 Trenberth, K.E. (2011). Changes in precipitation with climate change. *Climatic Research,* 47,
746 123-138. https://doi.org/10.3354/cr00953
747 Xia, Y., Hu, Y., & Liu, J. (2020). Comparison of trends in the Hadley circulation between
748 CMIP6 and CMIP5. *Science Bulletin,* 65, 1667–1674.
749 https://doi.org/10.1016/j.scib.2020.06.011
750 Xu, Y., Gao, X., & Giorgi, F.J. (2010). Upgrades to the reliability ensemble averaging method
751 for producing probabilistic climate-change projections. *Climate Research,* 41, 2375-2385
752 Yatagai, A., Kamiguchi, K., Arakawa, O., Hamada, A., Yasutomi, N., & Kitoh, A. (2012).
753 APHRODITE: Constracting a Long-Term Daily Gridded Precipitation Dataset for Asia Based
754 on a Dense Network of Rain Gauges. *Bulletin of the American Meteorological Society,* 93,
755 1401-1415. https://doi:10.1175/BAMS-D-11-00122.1
756 Yoo, J., & Rohli, R.V. (2016). Global distribution of Köppen–Geiger climate types during the
757 Last Glacial Maximum, Mid-Holocene, and present. *Palaeogeography, Palaeoclimatology,*
758 *Palaeoecology,* 446, 326–337. http://doi.org/10.1016/j.palaeo.2015.12.010